The Supercell Spectrum. Part II:
A Semi-Objective Method for Radar Classification of Supercell Type

KYLE BEATTY
Willis Re Inc.
Minneapolis, Minnesota

ERIK N. RASMUSSEN
Rasmussen Systems LLC
Mesa, Colorado

JERRY M. STRAKA
School of Meteorology
University of Oklahoma
Norman, Oklahoma

LESLIE R. LEMON
Cooperative Institute for Mesoscale Meteorological Studies and
NWS Warning Decision Training Branch
Norman, Oklahoma

(Submitted 03 March 2008; in final form 25 March 2009)

ABSTRACT

This paper describes a method for classifying supercells that relies partially upon a mixture of objective radar analysis and human analysis. The technique is used to ascertain the direction and distance of supercell precipitation core centroids from their updrafts. It is applied to a number of cases, and in this small sample the supercell centroids appeared to be segregated into locations upstream and downstream of the updraft, but not immediately beside the updraft. This suggests the spectrum of supercell precipitation morphologies may have modes that could be associated with the legacy categories of "HP" and "LP/Classic". Based on this analysis, we suggest that supercell classification be radar-based and utilize the classes "forward reflectivity mode" and "rear reflectivity mode".

1. Introduction

Part I (Beatty et al. 2008) presented a comprehensive review of the historical research related to the supercell spectrum. The evolution of terminology, and its basis in the precipitation structure, was discussed. The results of the literature review made it apparent that a considerable degree of subjectivity has existed in supercell classification, often depending on visual characteristics that changed with observer location. Part I also provided a motivation for researching a more objective approach to classification as it was shown that attendant weather phenomena can be associated with supercell type.

Part II herein explores an experimental technique for classifying supercells based on radar characteristics. Particular focus is placed on the displacement of the precipitation centroid with respect to the updraft, motivated by the broad visual classification approach that has been applied for many years. This approach has been made objective to the degree possible in a preliminary study. The authors believe it someday may be possible for applications engineers to make the technique fully objective and automated, but the exploration of automation is beyond the scope of this research

Corresponding author address:
E. N. Rasmussen, P.O. Box 267, Mesa, CO 81643. Email: rasm1@rasmsys.com

In Section 2, the methodology of the classification scheme is discussed. In Section 3, the technique is applied to a number of supercells with differing visual characteristics through large portions of their evolution life cycle. The findings are summarized in Section 4. A lengthy appendix is provided to illustrate the technique and allow the reader to attempt to duplicate the results, if desired.

2. Data and methodology

A semi-objective method for assessing the distribution of precipitation about a supercell's updraft is presented and tested for a sample of supercells. "Semi-objective" means that parts of the method rely on human assessment and other parts are completely automated. The general premise of the technique is to assess the distance separating the supercell updraft and its near-surface precipitation core. The analysis is conducted using Level II WSR-88D data within a modified version of the Map 1.02 software application, developed by E. Rasmussen (available upon request through the corresponding author).

a. Estimation of precipitation core location

The lowest radar elevation (0.5° scan) is used to estimate the location of the near-surface precipitation core. The analysis domain is limited to a range between 30-125 km. The 30 km threshold facilitates identification of features indicating the supercell updraft (described in the next section). The 125 km threshold limits the center of the base-scan radar beam to a maximum height of 2.0 km AGL. A closed polygon is defined around the supercell echo at the 0.5° elevation scan of each volume during the supercell's existence. The rain rate centroid R_c is estimated within the closed polygon assuming the Z-R relation (Vieux and Bendiet 1998);

$$Z = 0.01R^{0.833} \qquad (1)$$

where $10 \leq Z \leq 53$ dBZ. Only Z values in excess of 10 dBZ are considered, as lower values may be associated with index-of-refraction variations in the air rather than the cloud/precipitation field (Knight and Miller 1993). Note that other particulate matter (insects, birds, etc.) can increase Z. The Z is truncated at 53 dBZ, the default assumption used in semi-arid regions to reduce the hail bias in rain rate estimation (Vieux and Bedient 1998). The formulae used to calculate the centroid components R_{cx} and R_{cy} are

$$R_{cx} = \frac{\sum_{i=1}^{n} x_i R_i}{\sum_{i=1}^{n} R_i} \qquad (2)$$

$$\text{and } R_{cy} = \frac{\sum_{i=1}^{n} y_i R_i}{\sum_{i=1}^{n} R_i} \qquad (3)$$

and are further illustrated in Fig. 1. Other methods of estimating the location of the precipitation core were explored, such as weighting the centroid by a power of reflectivity or using a different Z-R relation (e.g., Marshall and Palmer 1948), however the WSR-88D Z-R relation was deemed adequate for this study. If supporting data are available, future calibration of the Z-R relationship may improve the analysis technique. A comparison of some of the methods for storm A from 13 June 1998 (Section 3c) is shown in Fig. 2.
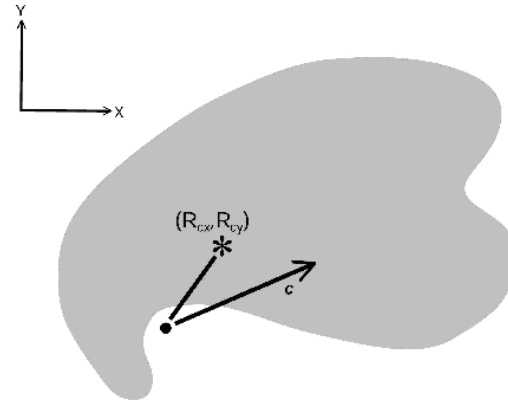

Figure 1. Conceptual illustration of the rain rate centroid relative to the storm motion vector. View is of the x-y plane. The black dot represents the extrapolated position of the supercell updraft at the map height. The asterisk represents the location of the rain rate centroid. C is the storm motion and speed.

When a supercell is not isolated (e.g., interacting with other convection or in the process of splitting into a left and right moving pair), the boundary of its echo may not be distinct. In such a case, the evolution of the three radar moments throughout the entire volume is studied to define individual cell boundaries and isolate those cells that merge with or propagate away from the supercell echo. This assessment is necessarily subjective.

Updraft Relative Echo Centroid Location
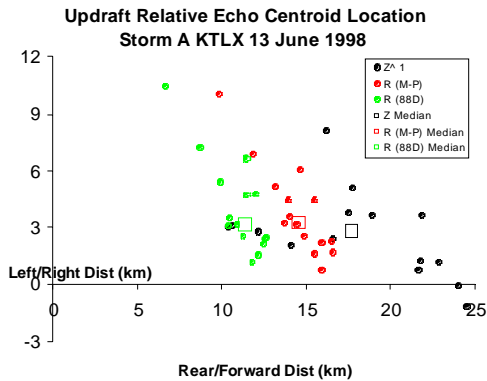**Storm A KTLX 13 June 1998**

Figure 2. Comparison of "echo centroid" calculation methods using weights based on 1) reflectivity Z, 2) rain rate R using a Marshall-Palmer distribution, and 3) R using the default formula for the WSR-88D in semi-arid regions. Squares represent medians for the three rain-rate assumptions.

b. Estimation of the low-level updraft location

Prior to the identification of features indicating the supercell updraft, the coordinates of the radar sample volumes are adjusted to remove the translation of echo associated with storm motion between elevation scans. Removal of this component of motion is important to estimate the tilt of the updraft axis properly, for later extrapolation to lower levels. Least squares linear regression of the coordinates (R_{cx}, R_{cy}) is used over the duration of the supercell's existence within the analysis domain to obtain mean storm motion c. The radar sample volume coordinates are adjusted per azimuth to the reference time associated with the average time of the 0.5° elevation scan and the time of the maximum elevation scan intersecting the supercell echo. The rain rate centroid coordinates also are adjusted using c for consistency with the reference time of each radar volume used in the updraft analysis.

The approximate axis of peak updraft velocity is identified subjectively at two or more elevation angles per radar volume. The detection of a bounded weak echo region (BWER) or vault in the mid-levels of a thunderstorm is a sufficient (but not necessary) condition for the identification of an organized updraft (Marwitz 1972a; Browning 1978). In some circumstances, the BWER will be evident at more than one elevation angle. Assuming updraft axis linearity,

the area of concavity that is bordered by the maximum reflectivity gradient and BWER should be aligned with the echo summit and area of maximum summit divergence aloft. The updraft also should be located on the inflow flank of a supercell's mesocyclone (Lemon and Doswell 1979). At upper levels, the vault will be overlain by strong reflectivity, which also can be used to approximate the updraft location (Lemon 1977). Additionally, if the radial is aligned with the low-level inflow, then the updraft should be marked in the velocity field by the conservation of low-level horizontal momentum (Lemon 1998). Finally, Lemon and Burgess (1993) and Lemon and Parker (1996) found evidence that the core of a thunderstorm updraft is predominately non-turbulent, detectable as a minimum of spectrum width through a significant depth of the storm. Since these features may not be identifiable at all ranges or stages within a supercell's life cycle, the four-dimensional radar presentation is considered for all three radar moments to establish time and height continuity of the estimated updraft axis.

The coordinates of the low-level updraft location $(r_{up\_low}, \theta_{up\_low})$ at the map height are estimated by using least squares linear regression of the coordinates of the identified mid- and upper-level updraft centers. The map height is defined as the curvilinear plane located 1.15 km above radar level. This height is chosen in order to minimize the error in distance between the extrapolated updraft axis and the cone of the 0.5° elevation scan between 30 and 125 km range (assuming wave propagation through the standard atmosphere). Once the low-level updraft location has been estimated, a quality check is performed to ensure that the point lies near a concave hook or pendant echo in the low-level reflectivity field, open to the sub-cloud winds and defined by a large, quasi-horizontal reflectivity gradient (Marwitz 1972b). Note that these features would not be present in a "true" low-precipitation (LP) supercell, as assessed from the radar perspective.

The coordinates of the extrapolated low-level updraft location are then projected onto a polar stereographic grid, consistent with method used to determine the Cartesian coordinates of R_c. The length of the ray between the estimated low-level updraft location and R_c, as well as the location of R_c relative to c then are determined.

*c. Assessment of the proximity storm relative
  flow*

As an application of the proposed technique to the problems discussed in Part I, the storm-relative flows in the mid- and upper-levels of the storm are assessed to determine possible relationships between the environment and the relative locations of the updraft and rain rate centroid. The low, middle, and upper levels are defined in a storm depth-relative reference frame, using a 30-40-30 percent division of the storm depth from the ground to the top of the anvil canopy (excluding the overshooting dome). To determine the storm depth, the height of the 10-20 dBZ reflectivity contours downstream of the echo top are measured. This process is repeated for each volume scan and the values are averaged to determine a mean storm height. The local elevation at each updraft track point is obtained using a Digital Elevation Model and these values are averaged to determine a mean ground elevation. For the cases examined herein, a mean ground elevation is a reasonable assumption, since the elevation gradient typically is small (~1-2 m km^{-1}) in the south-central Plains and the analysis domain limits a supercell track to < 200 km. If storms were analyzed over steeper terrain and/or if the analysis domain was expanded to include multiple radars, then use of a single elevation may not be appropriate.

Wind observations from NOAA's Wind Profiler Demonstration Network are used to characterize the middle and upper tropospheric flow since this observation platform has greater spatial and temporal resolution than the standard radiosonde observations. The system measures wind speed and direction at a vertical resolution of 250 m, with an average horizontal resolution of 250 km. Six minute observations are summarized into an hourly consensus mean value. If a consensus of at least 4 of the 10 observations is not obtained, then no observation is reported at that height. This processing scheme is employed to reduce the potential error caused by heterogeneities in the horizontal and vertical wind over the area formed by the zenith and off-zenith beams. A second quality check is completed by visually inspecting the hodograph for each of the reporting profiler stations to identify and exclude observations that are suspect or contaminated by convection.

Because filtering the data often results in uneven vertical observation spacing for a given profile and since the MSL elevation varies

significantly between individual sites, each wind profile is interpolated vertically to obtain wind estimates at 250 m MSL increments. A vertical wind profile then is estimated at the location of the extrapolated low-level updraft using a two-pass Barnes (1964) objective analysis scheme at each height increment. The analysis parameters g=0.3 and c=35000 were chosen such that wavelengths of 1250 km or greater were passed through the analysis virtually intact (Fig. 3).
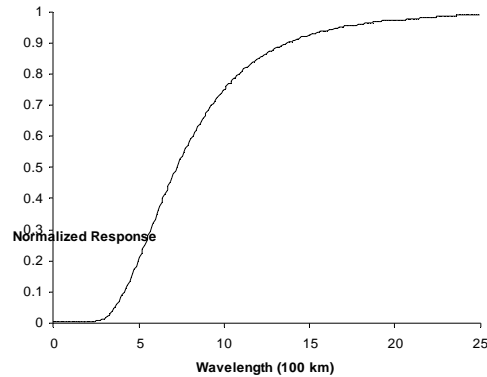

Figure 3. The response function after two passes of the Barnes analysis. The illustrated curve is for g=0.3 and c=35000. Wavelengths < 500 km are damped severely, whereas wavelengths greater than 1250 km are passed virtually intact.

The storm motion *c* is used to express the analyzed wind profile in the storm-relative reference frame. The component of the storm-relative wind vector in the direction of the rain rate displacement vector *R* is obtained using the formula

$$U_R = \vec{c} - \vec{R}_c \qquad (4)$$

The mean wind speed in the direction of this displacement vector is then obtained for the mid and upper storm-relative layers.

3. Supercell cases

a. Plainview storm of 25 May 1994

A storm located near Plainview, TX (hereafter referred to as the "Plainview storm") exhibited classical supercell characteristics as seen from the Lubbock, TX WSR-88D radar (KLBB) between 1957 and 2052 UTC. Although photographic evidence of this storm has not been located, it is included in this analysis since storms on this date near Lubbock were noted to exhibit visual LP characteristics (Rasmussen and

Straka 1998; hereafter RS98). The specific visual character of this particular storm, however, is not known. It also is included since it was within sufficient range of both the Amarillo, TX (KAMA) and KLBB radars to consider variation of analysis results when considering the perspective of different radars.

The Plainview storm traveled toward 074° at 15 m s^{-1} over the ~1 h analysis period. During the first 15 min of the analysis period, the storm possessed characteristics of a developing supercell weak echo region (e.g., WER, strong low-level reflectivity gradient, etc.). Over time, a BWER became evident and the high-level echo core began to shift to overlay the strong low-level reflectivity gradient. This indicates an intense updraft, given the range of 85-100 km from the radar.

Between 1957 and 2052 UTC, 12 radar volume scans from KLBB were suitable for updraft/rain rate centroid analysis. The reflectivity boundary of the supercell over the analysis period and the associated rain rate centroids are shown in Fig. A1[2]. By 2012 UTC, the storm was undergoing a division with a left member beginning to progress independently toward the north. This division required subjective determination of the time of split and delineation between cells up to 2227 UTC (cf. panels 3,4 of Fig. A1). A similar subjective decision was required during a merger of cells as a developing storm merged into the supercell's forward flank between 2027 and 2042 UTC (cf. panels 7-9 of Fig. A1).

There were additional challenges in updraft identification from 1957-2007 UTC, since a BWER was not evident. The determination of the low-level updraft location at this time was largely dependent on the detection of the echo top and echo core at upper and mid levels. If the supercell had been located at a different range and/or the volume coverage pattern did not allow detection of the echo top, the analysis may not have been possible at these times. In total, BWERs were well defined at multiple elevation angles in 8 of the 12 volume scans, providing high confidence in the inferred midlevel updraft location at these times. The resulting displacement between the extrapolated low-level

---

[2]To allow for coherent flow of text, the multi-panel radar reflectivity images are presented in the Appendix. The figures are included primarily to enhance the repeatability of the research.

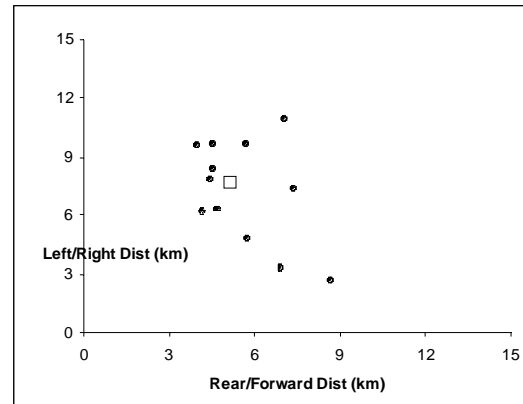updraft location and the rain rate centroid is summarized in Fig. 4.

Figure 4. Displacement of the rain rate centroid relative from the updraft (dots) for the Plainview storm. The median value is depicted as an open square. The coordinate system has been rotated such that the direction of storm motion is oriented toward the east (right).

b. "Storm B" from 3 May 1999

Storm B from 3 May 1999 (Speheger et al. 2002) was analyzed for the 2.75 h it existed within the range criteria of scans, providing high confidence in the inferred mid-level updraft location at these times. The resulting displacement between the extrapolated low-level updraft location and the rain rate centroid is summarized in Fig 4.

In the mean, the rain rate centroid was located 9 km north-northeast of the storm's updraft. The top of the Plainview storm's anvil shield was estimated to be at 11.5 km AGL, placing the middle layer at 4-8.25 km and the upper layer at 8.25-11.5 km. The SR winds were substantially stronger in the upper region of this storm as compared to mid levels (average of 11 m s^{-1} greater). The difference in the SR winds between these levels exceeds that of other storms analyzed in this sample. The component of the winds in the direction of the updraft/rain rate centroid displacement was greater on average by 15 m s^{-1} in the upper storm layer (see Fig. 5). As previously noted, this supercell exhibited some visual features of an LP supercell early in its existence, evolving into a more classic supercell appearance. Between 2332 and 0216 UTC, 32 radar volume scans from Oklahoma City (KTLX) were suitable for updraft/rain rate centroid analysis. The reflectivity boundary of
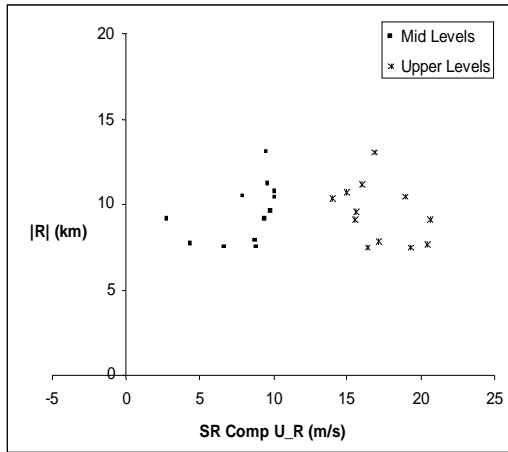
Figure 5. Magnitude of the storm relative wind *UR* in the direction of the Plainview storm's rain rate centroid displacement vector **R** (tail at low-level updraft and head at the rain rate centroid; ordinate) versus the magnitude of rain rate centroid displacement vector /**R**/.
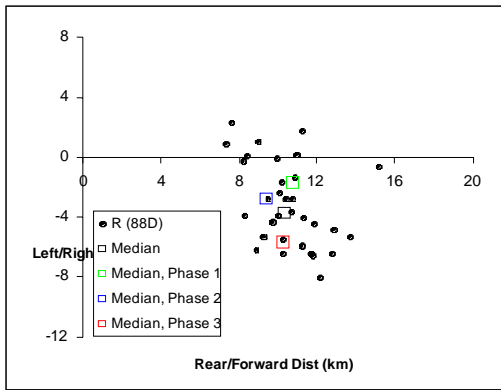

Figure 6. As in Fig. 4 but for storm B, 3 May 1999. The evolution of the rain rate centroid displacement is illustrated in phases 1-3 for 2332-0022, 0027-0117, and 0121-0216, respectively.
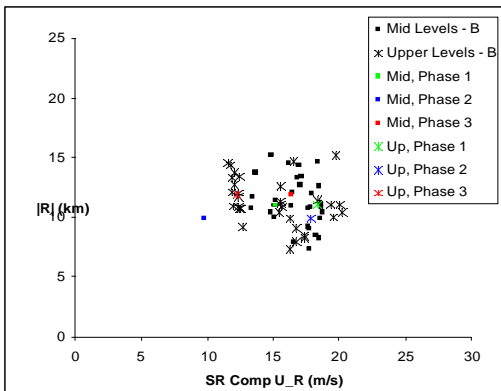

Figure 7. As in Fig. 5 but for storm B, 3 May 1999. Phases follow Fig. 6.

the supercell over the analysis period and the associated rain rate centroids are shown in Fig. A2. The storm remained isolated over the analysis period, leaving very little subjectivity in the definition of storm boundary.

Updraft identification was relatively straightforward with this storm, often exhibiting a BWER at multiple elevation angles. This was particularly true as the storm passed within 50 km to the northwest of KTLX. The resulting displacement between the extrapolated low-level updraft location and the rain rate centroid is summarized in Fig. 6. The mean rain rate centroid was located 11 km east-northeast of the storm's updraft. Of particular interest in this case is the temporal evolution of **R**. Interestingly, the distance from the updraft location did not change appreciably over the analysis period, despite the visual observations that the storm evolved from a more LP to a classic visual appearance (cf. Fig. A2). The centroid location did migrate approximately 4 km further to the right of the storm motion vector over time.

The top of storm B's anvil shield was estimated at 11.9 km AGL, yielding the depths of 3.5-8.3 km and 8.3-11.9 km for the middle and upper storm layers, respectively. The SR winds weakened with time in both the mid and upper layers. The rate of weakening was greatest in the upper layer, with the mid layer having slightly greater winds than the upper layer at the end of the analysis period (Fig. 7). The magnitude |**R**| also was observed to remain relatively constant over time, despite the weakening of the winds aloft.

c. "Storm A" from 13 June 1998

Two of the three supercells that existed within the KTLX analysis domain on 13 June 1998 were studied. The third storm was not investigated since it moved directly over the radar site, precluding analysis continuity (visible to the southwest of storm B in Fig. A4, panels 12-19). The first storm, hereafter referred to as storm A, entered the domain at 2209 UTC near Watonga, OK. The storm was already well organized at this time, exhibiting radar characteristics of a supercell (i.e., mesocyclone signature, BWER, low-level concavity in reflectivity field, etc.). The storm exhibited these features until it began to weaken northeast of Guthrie, OK around 0000 UTC 14 June 1998.

Figure 8. Photo of storm A from 13 June 1998 at 2332 UTC. The photographer was located to the south of the storm's reflectivity maximum looking toward the northwest at the storm's mesocyclone. (Photo courtesy Michael Magsig)

The storm exhibited visual characteristics of an LP supercell over this period (Fig. 8). Note though the heavy precipitation under the updraft base to the rear (northwest) of the storm. At approximately 2326 UTC, the storm was observed to produce a warm, precipitation-free rear flank downdraft (J. LaDue, personal communication), indicating that any associated precipitation likely evaporated aloft. Between 2209 and 2350 UTC, 15 radar volume scans from KTLX were suitable for updraft/rain rate core analysis. During the first 75 min of this analysis period, there were several additional cells located to the north of storm A, resulting in overlapping radar echoes at the 0.5° elevation. Cells that were identified subjectively as being independent of the supercell were excluded from the calculation of the rain rate centroid (e.g. panels 1-8 of Fig. A3).

Other analysts may interpret the reflectivity field differently, resulting in different locations of the rain rate centroid. The uncertainty associated with this component of the analysis is generally small, since periphery cells typically have low reflectivity and $R=Z^{1.2}$. The reflectivity boundary of the supercell over the analysis period and the associated rain rate centroids are shown in Fig. A3.

BWERs were well defined at multiple elevation angles for nearly all volume scans, providing reasonably high confidence in the inferred mid-level updraft locations for this storm. The displacement between the extrapolated low-level updraft location and the rain rate centroid is summarized in Fig. 9. In the mean, the rain rate centroid was located 12 km east-northeast of the storm's updraft. The upper-level SR winds averaged 6 m s^{-1} stronger than

those in midlevels, and veered with time, whereas midlevel winds were steadier. The component of the winds in the direction of the updraft/rain rate centroid displacement was greater on average by 5 m s^{-1} in the upper storm layer (Fig. 10).
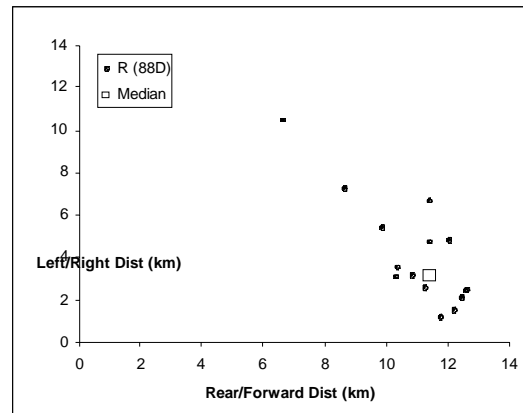

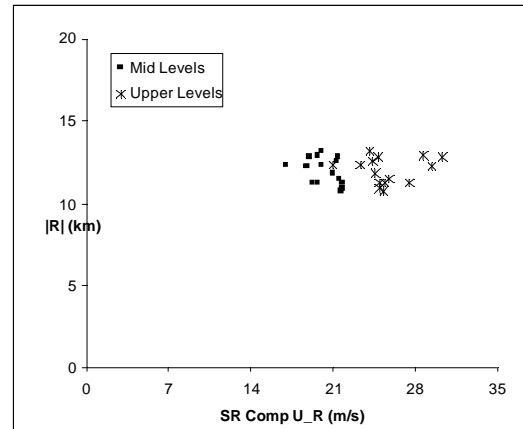Figure 9. As in Fig. 4 but for storm A, 13 June 1998.

Figure 10. As in Fig. 5 but for storm A, 13 June 1998.

Figure 11. Photo of storm B from 14 June 1998 at 0100 UTC. The photographer was located below the storm's weak echo region looking northwestward at the mesocyclone. (Photo courtesy of Michael Magsig)

d. "Storm B" from 13 June 1998

The second storm analyzed from 13 June 1998, hereafter referred to as storm B, entered the domain at 2345 UTC north of Hinton, OK. Similar to storm A, this storm was well organized at the time, exhibiting radar characteristics of a classic supercell. The storm maintained these features until it began to weaken east of Arcadia, OK around 0145 UTC 14 June 1998.

The reflectivity boundary of the supercell over the analysis period and the associated rain rate centroids are shown in Fig. A5. The analysis began after storm A had divided into a left and right moving pair, and therefore there was little ambiguity of the storm's reflectivity boundary.

The storm had a prominent vertical updraft, heavy rain downstream of the updraft, and strong rear flank downdrafts consistent with the classic supercell archetype (J. LaDue, personal communication; Fig. 11).

Over its two hour period in the analysis domain as a supercell, 18 radar volume scans of storm B from KTLX were suitable for updraft/rain rate centroid analysis. Unlike storm A, storm B remained isolated throughout the analysis period except for smaller radar echoes that merged with the storm from the south. The role of the mergers is not known. The displacement between the extrapolated low-level updraft location and the rain rate centroid was computed from the data in Fig. A4. In the mean, the rain rate centroid was located 11 km north-northeast of the storm's updraft (Fig. 12).

Initially, the SR winds in the mid levels of storm B were slightly stronger than those observed in the upper layer of the storm. The upper level winds strengthened and veered with time to be over 8 m s^{-1} stronger than the mid

levels at the end of the analysis period. The component of the winds in the direction of the updraft/rain rate centroid displacement was greater on average by 6 m s^{-1} in the upper storm layer (Fig. 13)

e. "Storm A" from 3 May 1999

Storm A from 3 May 1999 was analyzed for the 1.8 h it existed within the range criteria from KTLX. As previously noted, it generally exhibited visual and radar features of a classic supercell. Between 2139 and 2327 UTC, only 11 radar volume scans from KLTX were suitable for updraft/rain rate centroid analysis. Several scans over this period had missing data due to radar system failure. The supercell also persisted for over an hour after the termination of the analysis, as it progressed over the radar site.
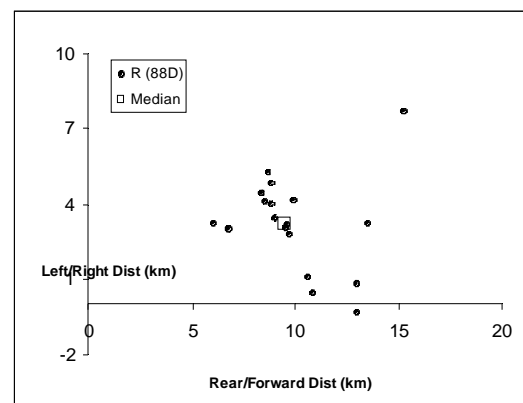

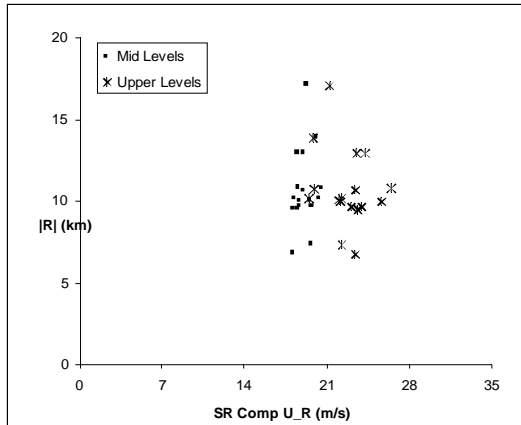Figure 12. As in Fig. 4 but for storm B, 13 June 1998.

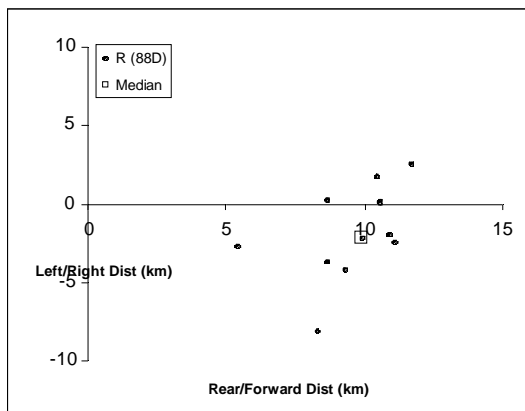Figure 13. As in Fig. 5 but for storm B, 13 June 1998.

Figure 14. As in Fig. 4 but for storm A, 3 May 1999.

The identification of the updraft was relatively straightforward with this storm, which often exhibited a BWER at multiple elevation angles. This was particularly true as the storm neared the KTLX radar. The resulting displacement between the extrapolated low-level updraft location and the rain rate centroid is summarized in Fig. 14. In the mean, the rain rate centroid was located 10 km northeast of the storm's updraft. The height of storm A's anvil shield was the same as that of storm B, previously described. The SR winds were substantially stronger in the upper levels as compared to the mid levels of storm A [Fig. 15 similar to phase 1 of storm B (cf. Fig. 7)].

f. Near Lubbock, 25 May 1999

The storm exhibited the visual and radar characteristics of a heavy-precipitation (HP) supercell as it moved toward 128° at 11 m s^{-1} (C. Doswell, personal communication; Fig. 16). The storm had a well-defined, expansive gust front extending off to its southeast.

Between 2156 and 2251 UTC, 11 radar volume scans from KLBB were suitable for updraft/rain rate centroid analysis. The reflectivity boundary of the supercell over the analysis period and the associated rain rate centroids are shown in Fig A6. Cells that developed along the gust front to the storm's southwest were excluded from the rain rate centroid analysis. Similarly, the reflectivity associated with the gust front was excluded.
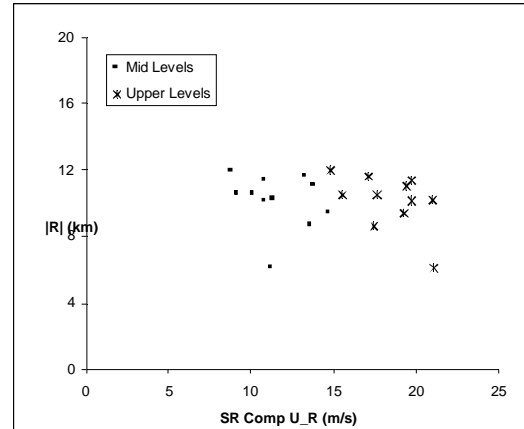

Figure 15. As in Fig. 5 but for storm A, 3 May 1999.

Figure 16. Photo of an HP supercell taken from north of Petersburg, TX near 2244 UTC on 25 May 1999. (Photo © C. Doswell, used by permission.)

Unlike the LP and classic storm examples, the rain rate centroid of this storm remained to the rear of the updraft throughout its duration (Fig. 17). Substantial reflectivity is present on the updraft's left, rear, and right quadrants, with the most expansive region on the left flank. As a result, *R* is in the second quadrant when viewed in the SR frame, as opposed to the first and fourth quadrants that were observed for classic

and LP storms. Also, $|\mathbf{R}|$ was slightly less in this case than the classic and LP cases. The environmental flow in proximity to the storm was relatively weak (centered on about 5 m s^{-1} in Fig. 18) in both the middle and upper layers, however, the winds were oriented in the opposite direction of $\mathbf{R}$.
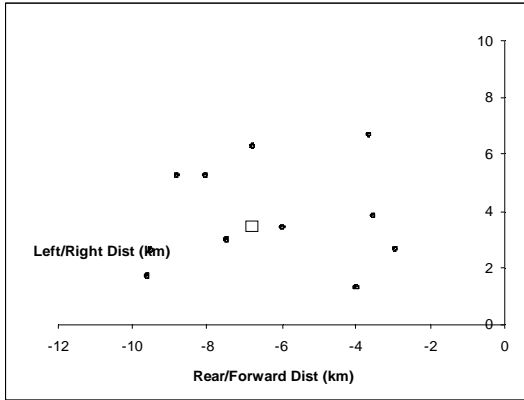

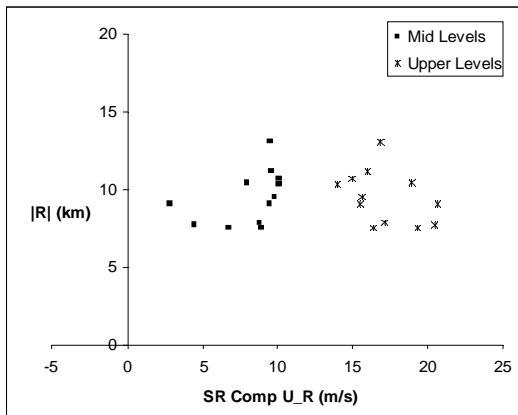Figure 17. As in Fig. 4 but for storm north of Lubbock, TX on 25 May 1994.

Figure 18. As in Fig. 5 but for storm north of Lubbock, TX on 25 May 1994.

g. Kaw Reservoir storm, 6-7 May 1994

The Kaw Reservoir storm was long-lived, exhibiting visual and radar characteristics of an HP supercell between 0128-0546 UTC on 7 May 1994 at it passed to the west of Tulsa, OK (KINX). This was the longest duration storm studied, with 45 radar volume scans suitable for analysis. The storm moved toward 160º at 10 m s^{-1}, from north-central Oklahoma to near Interstate 40. Unlike other cases assessed herein, the Kaw Reservoir storm was monitored using volume coverage pattern 21, which only includes nine scans per volume. The data voids between 4.3º and 6.0º elevation and 6.0º and 9.9º elevation in particular make detection of the

supercell echo top and BWER difficult. As a result, a greater weight had to be placed on other features such as the inflow flank of the mesocyclone and/or the maximum reflectivity gradient bordering the WER for some scans. In addition, a second supercell with approximately the same storm motion persisted immediately to the west of the Kaw Reservoir storm, resulting in overlapping low-level echo boundaries (Fig. A7). A top-down assessment of the reflectivity field was used to isolate the respective cells and define an approximate boundary between the two storms for each radar volume.

The displacement between the extrapolated low-level updraft location and the rain rate centroid is summarized in Fig. 19. In the mean, the rain rate centroid was located 6 km northeast of the storm's updraft. With a storm motion toward the south-southeast, this placed the rain rate centroid behind the storm's updraft, similar to the previous case. Although variable, the SR winds in the mid and upper levels were of similar magnitude, with the upper level winds perhaps stronger. (Fig. 20).
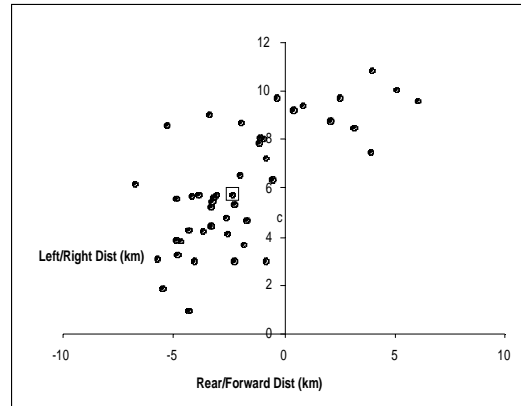

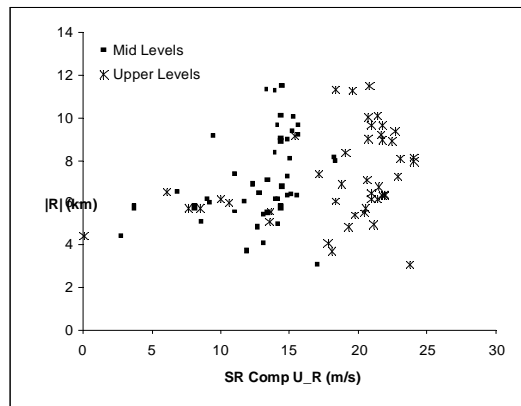Figure 19. As in Fig. 4, but for Kaw Reservoir storm on 6 May 1994.

Figure 20. As in Fig. 5, but for Kaw Reservoir storm on 6 May 1994.

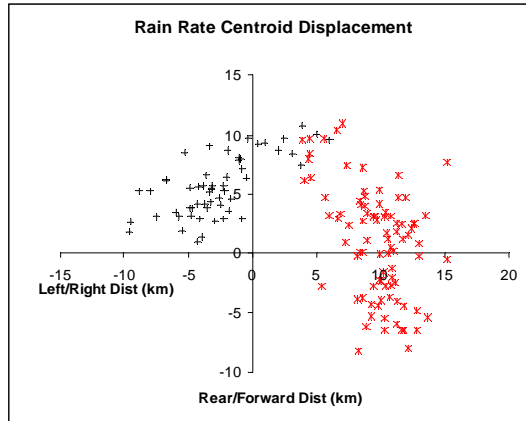**Rain Rate Centroid Displacement**

Figure 21. Updraft relative rain rate centroid locations for all cases. Storms with an LP/Classic visual appearance are shown with red "*", while those with HP visual appearances are shown with black "+".

The subjectivity of excluding non-supercellular echoes was described earlier. This particular instance poses additional concerns since 1) the dominant updraft of the convective system may vary frequently between cells in this type of multicellular convective system; and 2) each cell consists of high reflectivity, and therefore, improper exclusion of any one cell could lead to significant errors in the rain rate centroid estimation.

4. Discussion and conclusions

Despite its simplicity and the issues related to range and resolution with weather radar, the location of the rain rate centroid relative to the storm motion vector seems to be a fairly robust method to distinguish between storms with visual classical/LP and HP appearances (Fig. 21). Storms with LP or classic visual appearance have radar-derived low-level rain rate centroids in the forward flank, while storms with HP visual character have low-level rain rate centroids in the rear flank. This finding is intuitive and consistent with the description of HP supercells, which often evolve from the classic to HP state with an increased amount of precipitation on the rear side of the updraft. The findings from this sample indicate that there *may* be two dominant convective modes for supercells, whereby storms maintain most precipitation either in the front or rear flanks. It is also possible that a larger sample would place more data points between the two fairly discrete neighborhoods shown in Fig. 21, and hence a more continuous spectrum of centroid displacements.

It is possible that "true" LP storms that have no precipitation in the low levels of their rear flanks might have greater separation distances that would make these storms distinct. On the other hand, perhaps such storms do not exist; perhaps all supercells have some radar detectable precipitation in the rear flank but it is not visually apparent to the observer in the field.

Those storms that have classical radar appearances seem to have very similar rain rate centroid separation distances, regardless of their visual character (e.g., storms A and B on 13 June 1998 and the evolution of storm B on 3 May 1999). Although not critical in this case set, in a larger sample it would be necessary to stratify results by storm depth, since storms that are shallower inherently will inherently have shorter separation distances because of their smaller spatial scale.

Based on this research, we recommend that precipitation classification of supercells be done consistently via radar, and not visual appearance, when the storm is within sufficient range. Visual appearances are subjective, and therefore frequently lead to conflicting conclusions. We suggest using the terms "forward reflectivity mode" and "rear reflectivity mode" to distinguish between supercells viewed on radar. We further suggest that this quasi-objective approach for characterizing supercell precipitation variants be applied consistently to a larger sample of storms, to support or refute anecdotal evidence of favored degrees of severity within different archetypes.

In addition, based on the foregoing analysis, there appears to be a predictive signal in the SR winds at mid (Fig. 22) and upper levels (Fig. 23) in the proximity environments between the forward reflectivity mode and the rear reflectivity mode. (The reader is referred to Part I of this paper for an extensive discussion of the role of storm relative flow in supercell type.) The findings of this study are reasonably consistent with those of RS98 as well as Brooks et al. (1994). Although there is some overlap between classes, when mid-level flow exceeded ~18 m s^{-1}, the storms generally were in the forward reflectivity mode. Below about 8 m s^{-1}, the structure tended to be a rear reflectivity mode. Similarly with the upper level flow, forward reflectivity mode storms were not found below about 12 m s^{-1} storm-relative flow magnitude, and rear reflectivity mode storms were not found

when SR flow exceeded about 24 m s^{-1}. The use of a SR depth for evaluating the proximity environment seems to be important when strong vertical shear exists. It may be worthwhile to investigate the relationship between the rain rate centroid location and an adapted deep bulk Richardson number (DBRN) parameter (RS98), where the depth over which the magnitude of the shear vector is calculated is determined on a per-storm basis.
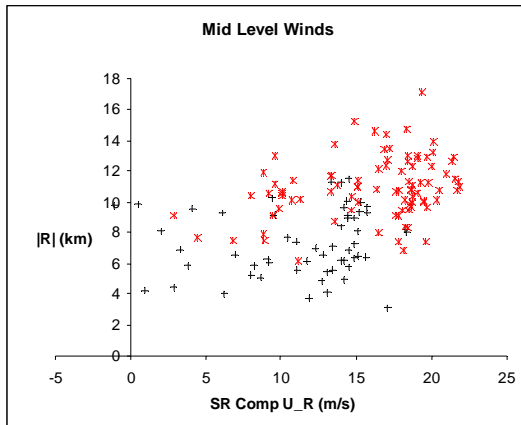

Figure 22. Mid-level SR winds only for all cases. Storms with an HP radar appearance are shown in black, while storms with a classical radar appearance are shown in red.
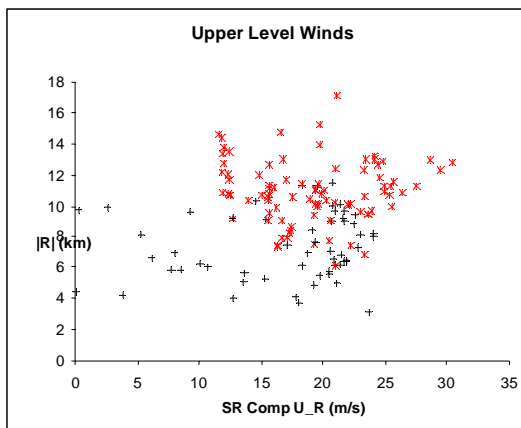
Figure 23. Upper-level SR winds only for all cases. Storms with an HP radar appearance are shown in black, while storms with a classical radar appearance are shown in red.

In conclusion, this paper provides evidence that supercells can be classified based on radar characteristics into two broad classes: forward reflectivity mode and rear reflectivity mode. These modes appear to be related to storm-relative flow in the supercell environments. We believe that these two broad findings should provide motivation in perhaps the somewhat distant future for attempts at automated radar-based storm type classification.

ACKNOWLEDGMENTS

APPENDIX

This appendix contains images of radar reflectivity, annotated with the boundary used to control the automated computation of the echo centroid, which is denoted with a black dot. The label next to the black dot contains information used by the analyst for record-keeping and is not of relevance to this paper. The purpose of the appendix is to allow others attempting to repeat this work to make sure that the same storms are being analyzed.

Join the Discussion

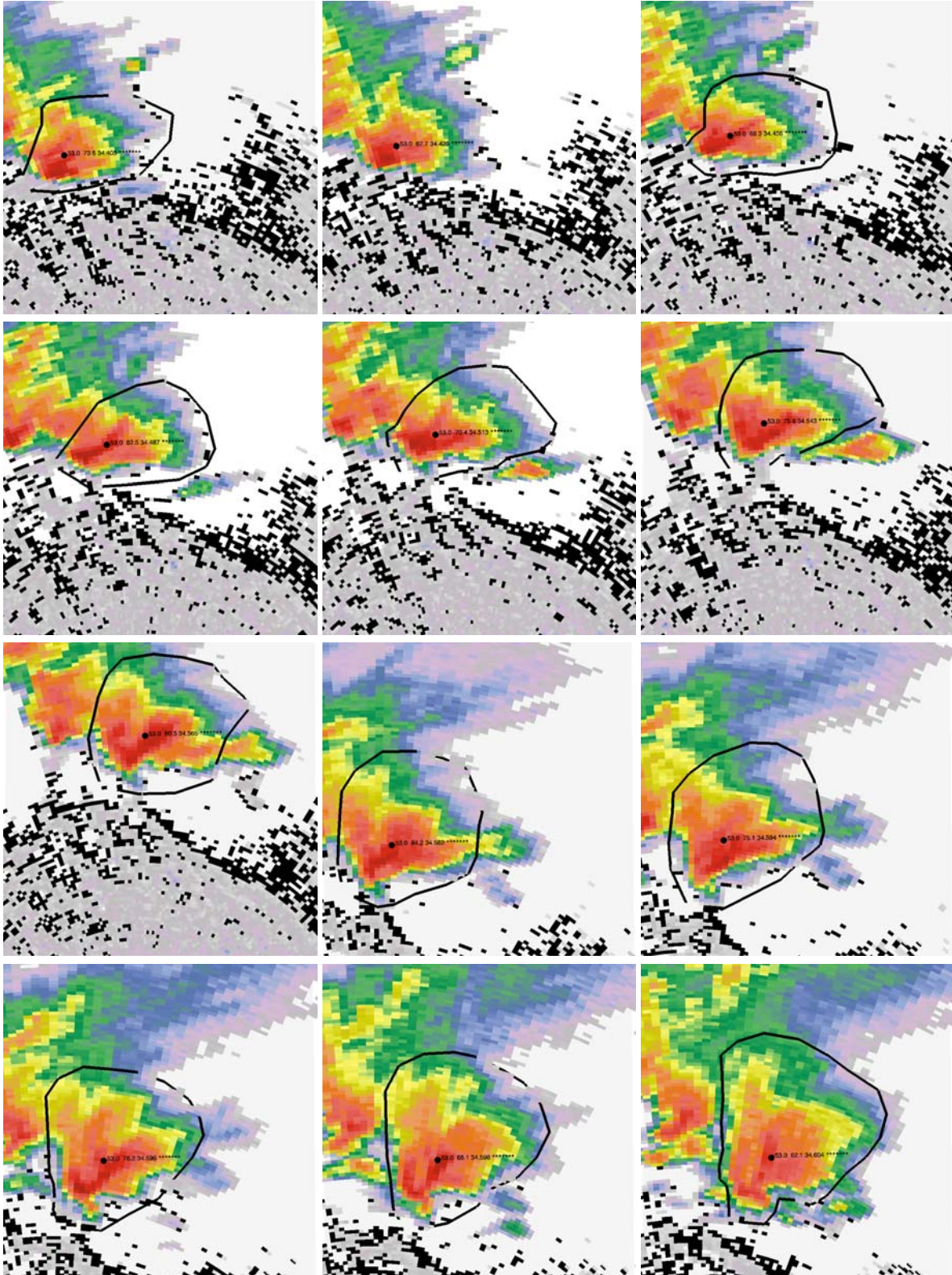Comments and discussion regarding this article are welcome at www.ejssm.org/forums.

Figure A1. Reflectivity analysis plots for the Plainview storm on 25 May 1994 from the KLBB WSR-88D radar. Rain rate centroids are depicted with a dot and are labeled from left to right identifying the maximum reflectivity, average reflectivity, latitude, and longitude at the map height of 2.16 km. References to panels in the text refer to panels counted from left to right and then top to bottom.
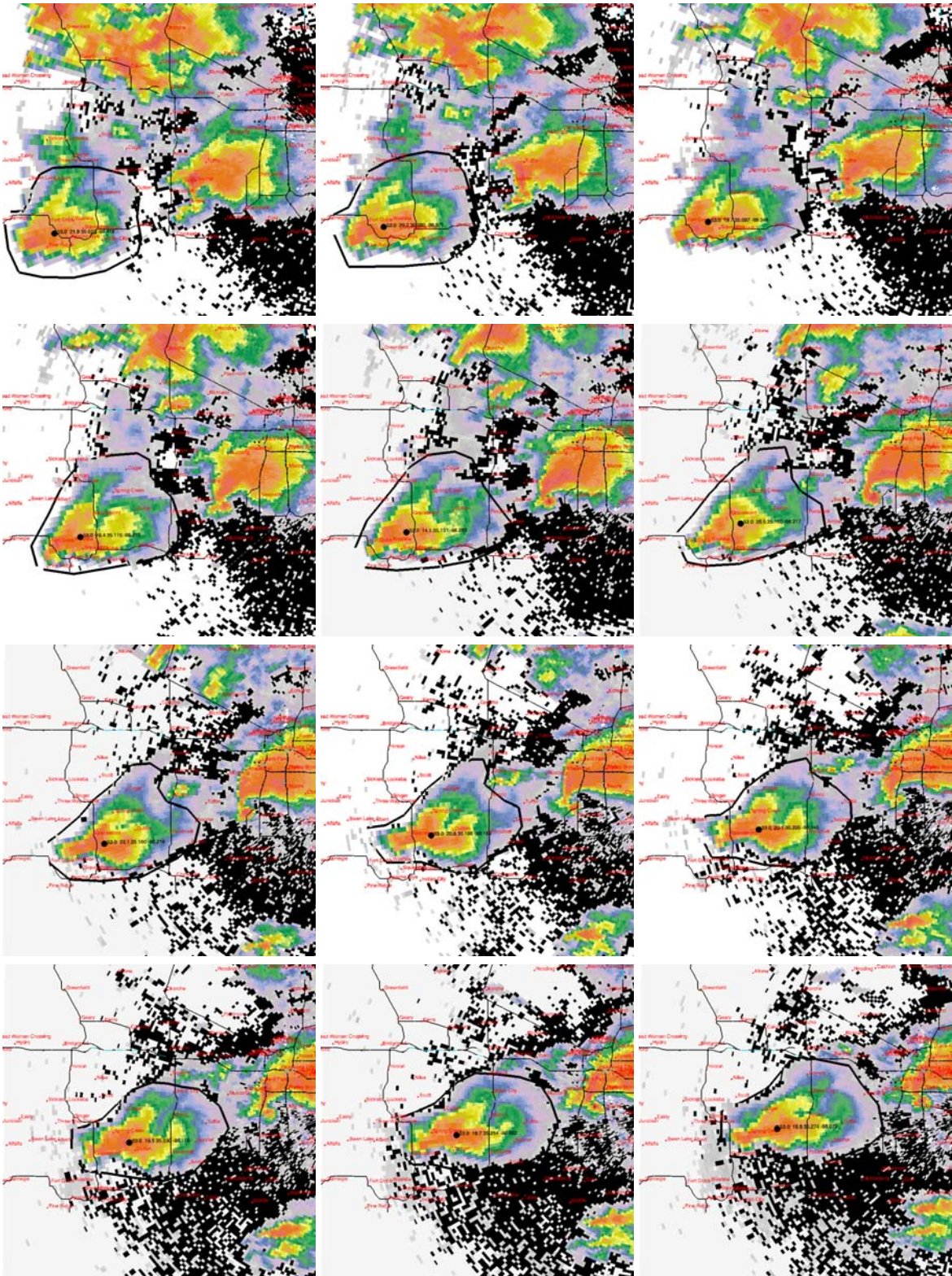
Figure A2. As in Fig. A1 but for storm B, 3 May 1999 viewed from KTLX between 2337 and 0107 UTC, for panels 1-12, respectively. Map height is 1.535 km AGL.
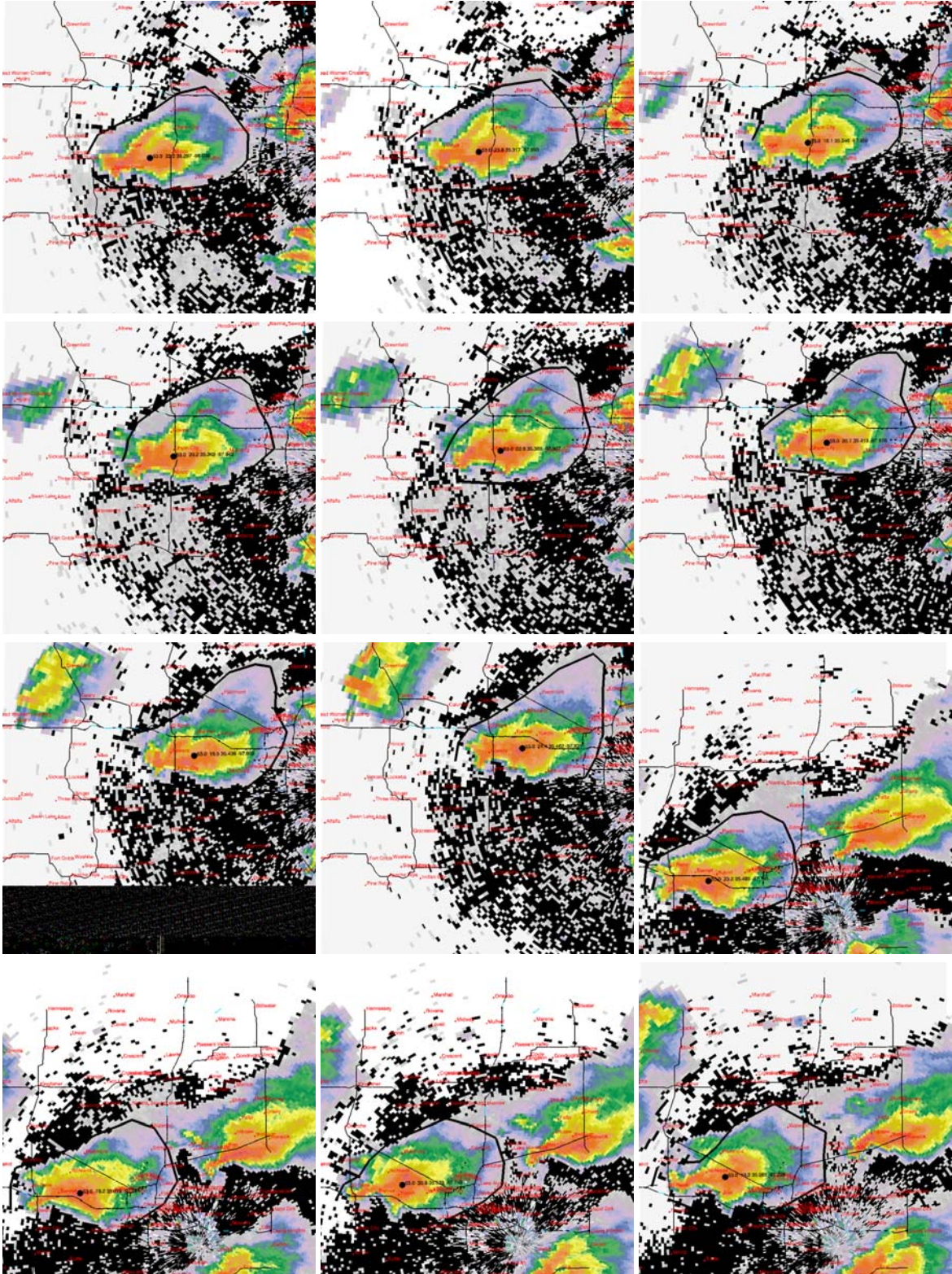
Figure A2. Continued. Panels 13-24.
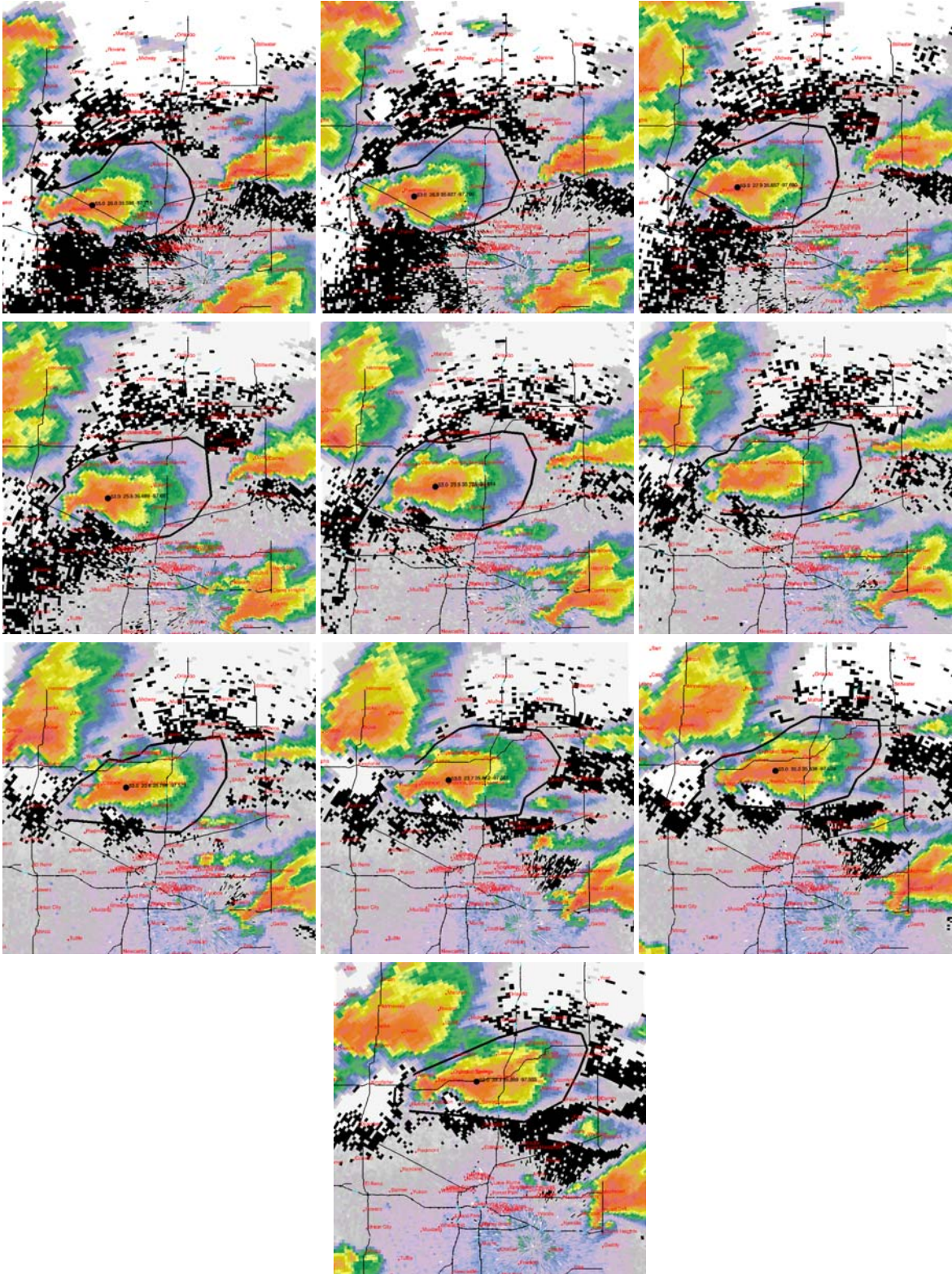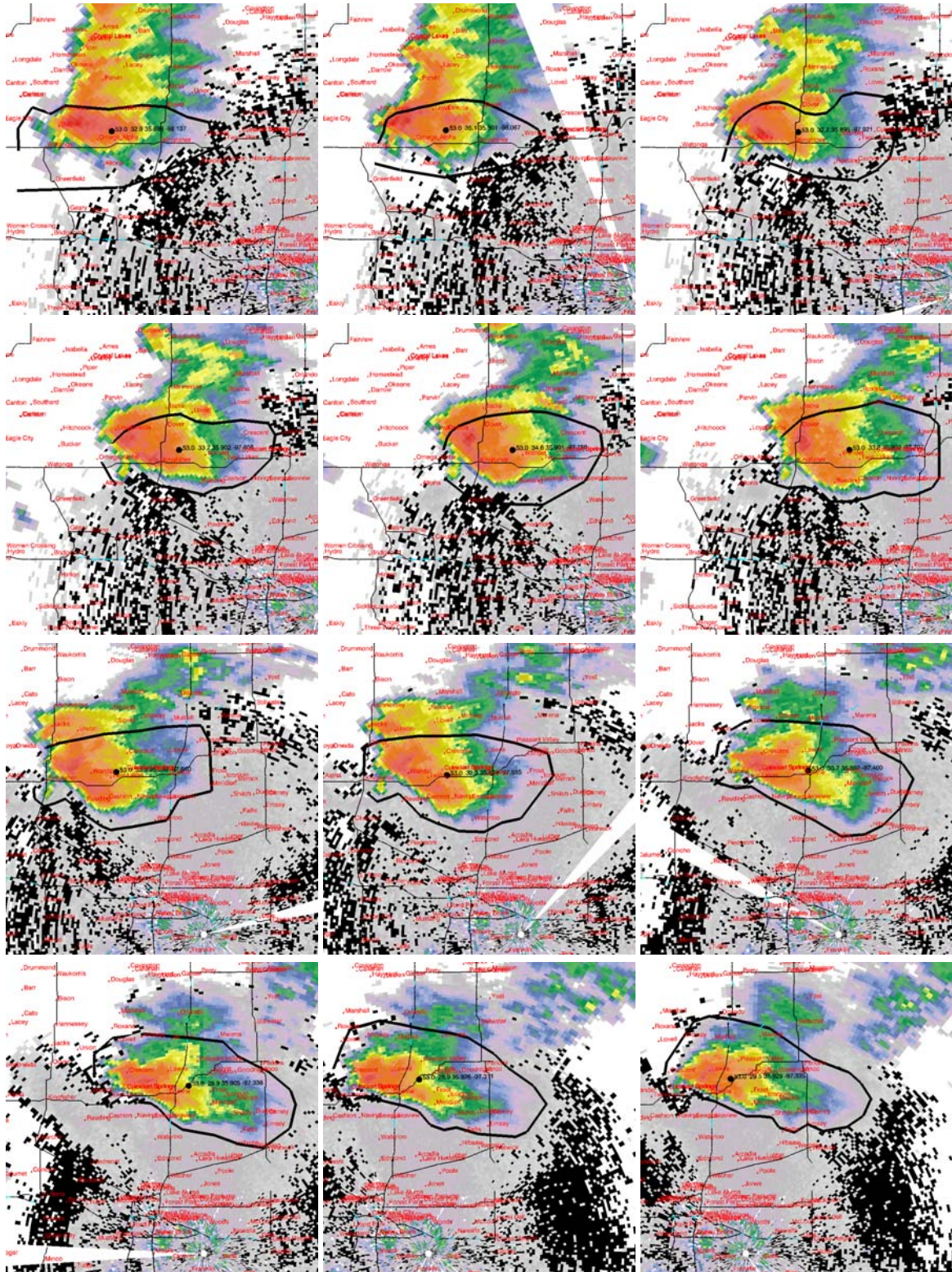
Figure A2. Continued. Panels 25-34.

Figure A3. As in Fig. A1 but for storm A, 13 June 1998, viewed from KTLX between 2209 and 2351 UTC, for panels 1-12, respectively. Map height is 1.535 km AGL.
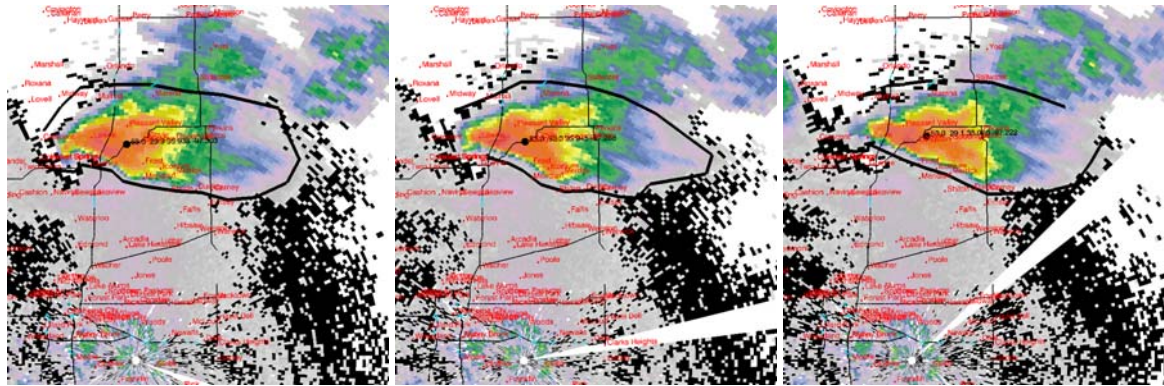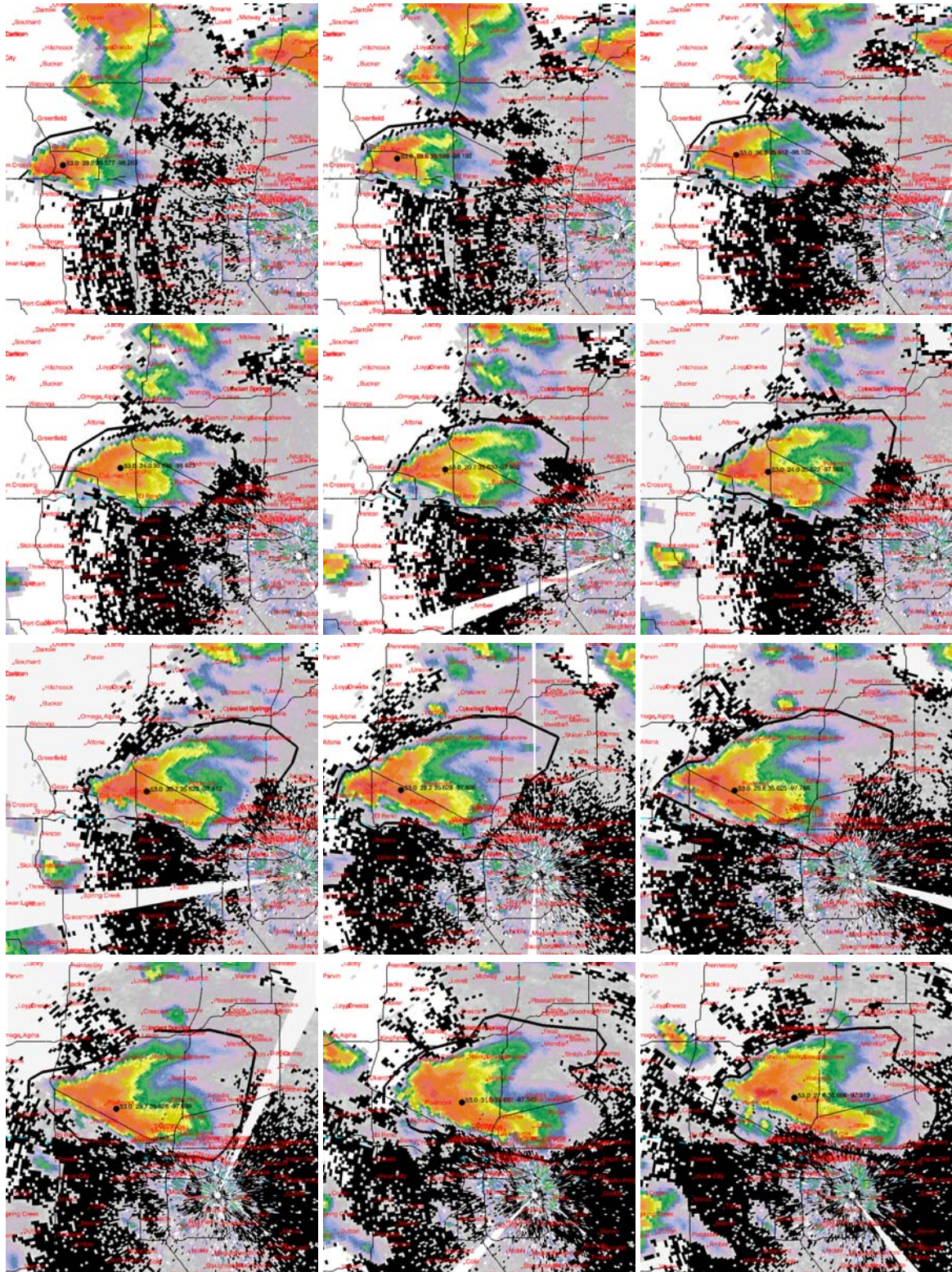
Figure A3. Continued. Panels 13-15.

Figure A4. As in Fig. A1 but for storm B, 13 June 1998, viewed from KTLX between 2345 and 0148 UTC, for panels 1-12, respectively. Map height is 1.535 km AGL.
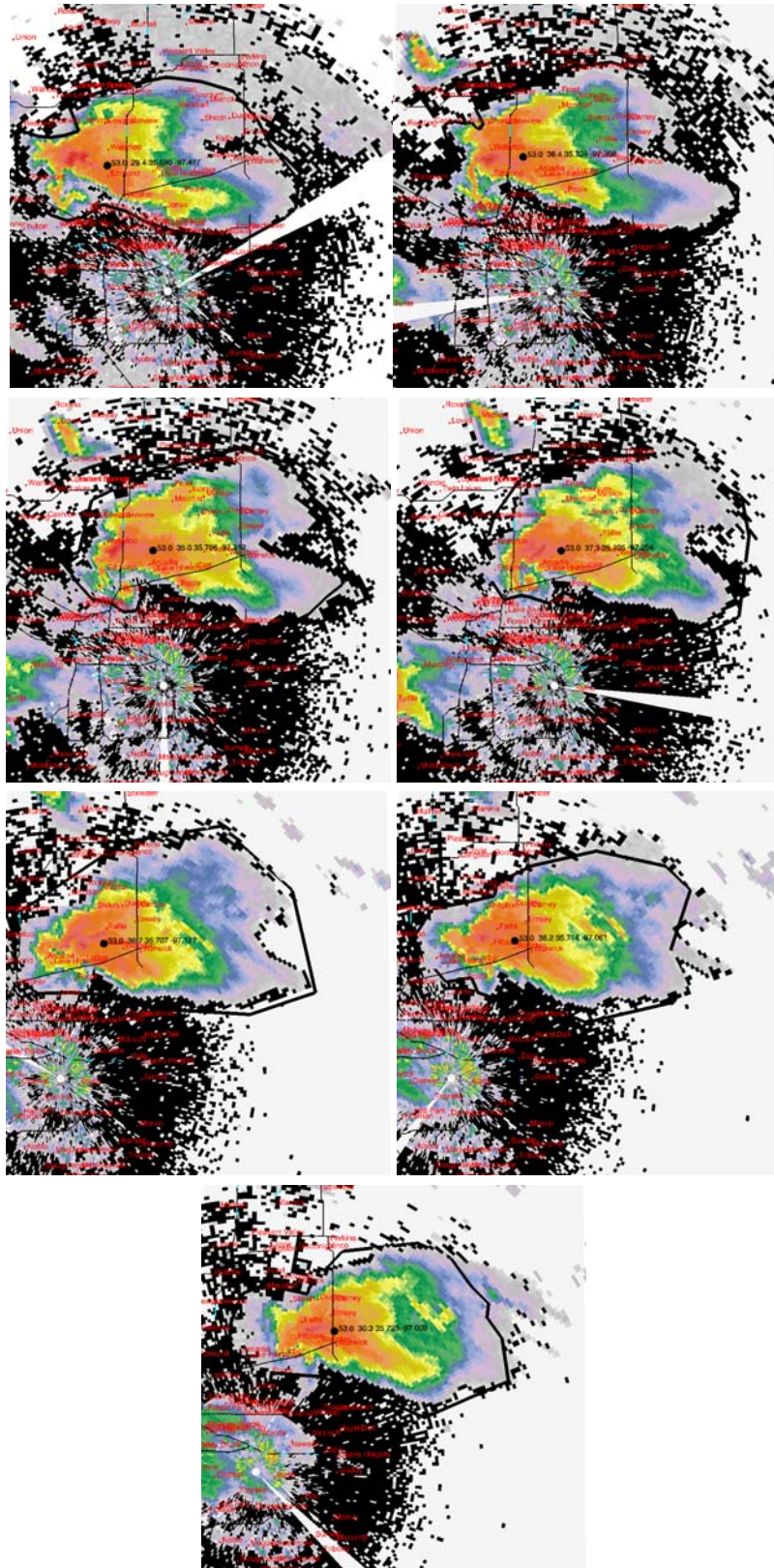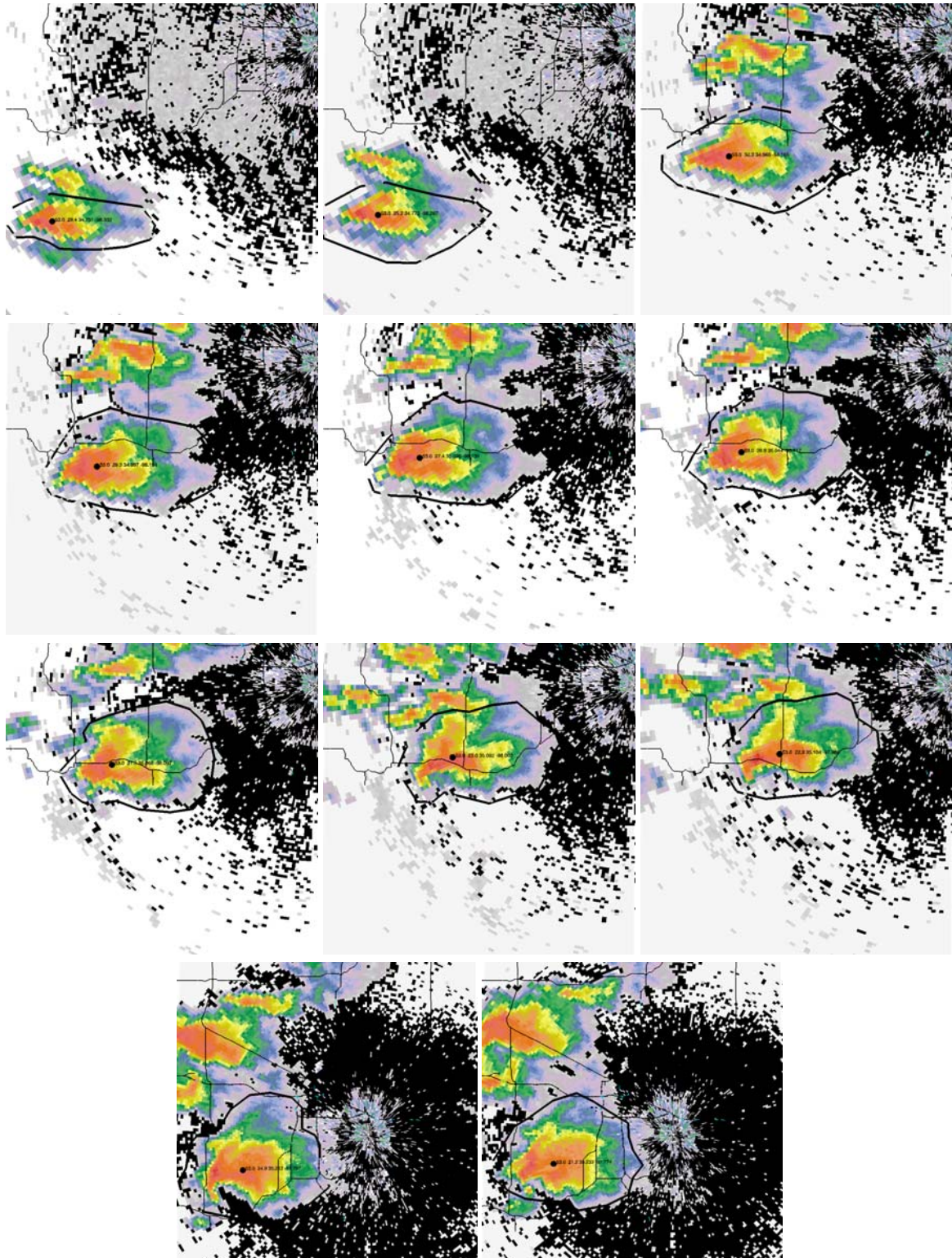
Figure A4. Continued. Panels 13-19.

Figure A5. As in Fig. A1, but for storm A, 3 May 1999, viewed from KTLX between 2139 and 2327 UTC, for panels 1-11, respectively. Map height is 1.535 km AGL.
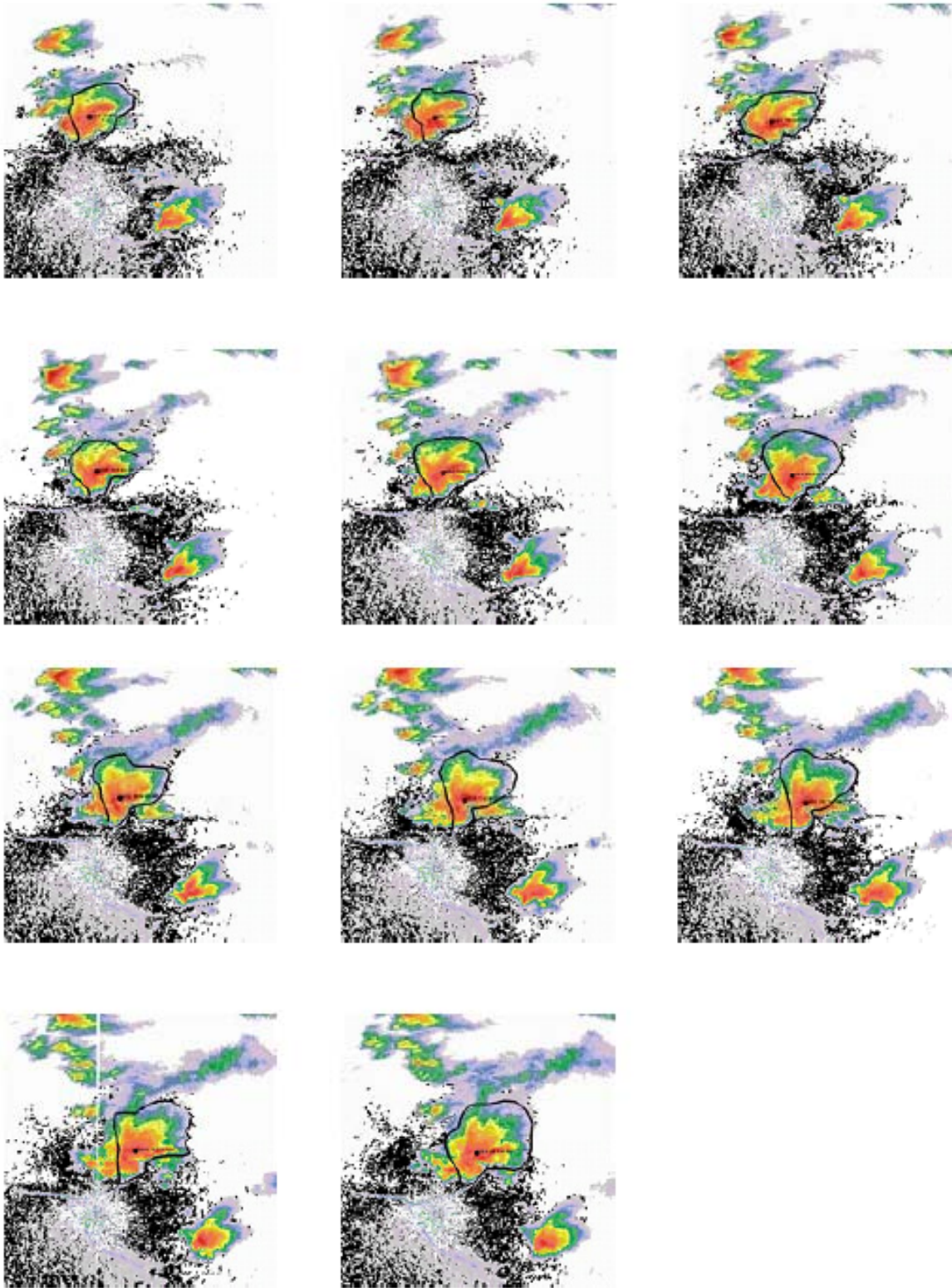
Figure A6. As in Fig. A1, but for the storm north of Lubbock, TX, on 25 May 1999, viewed from KLBB between 2156 and 2251 UTC for panels 1-11, respectively. Map height is 2.163 km AGL.
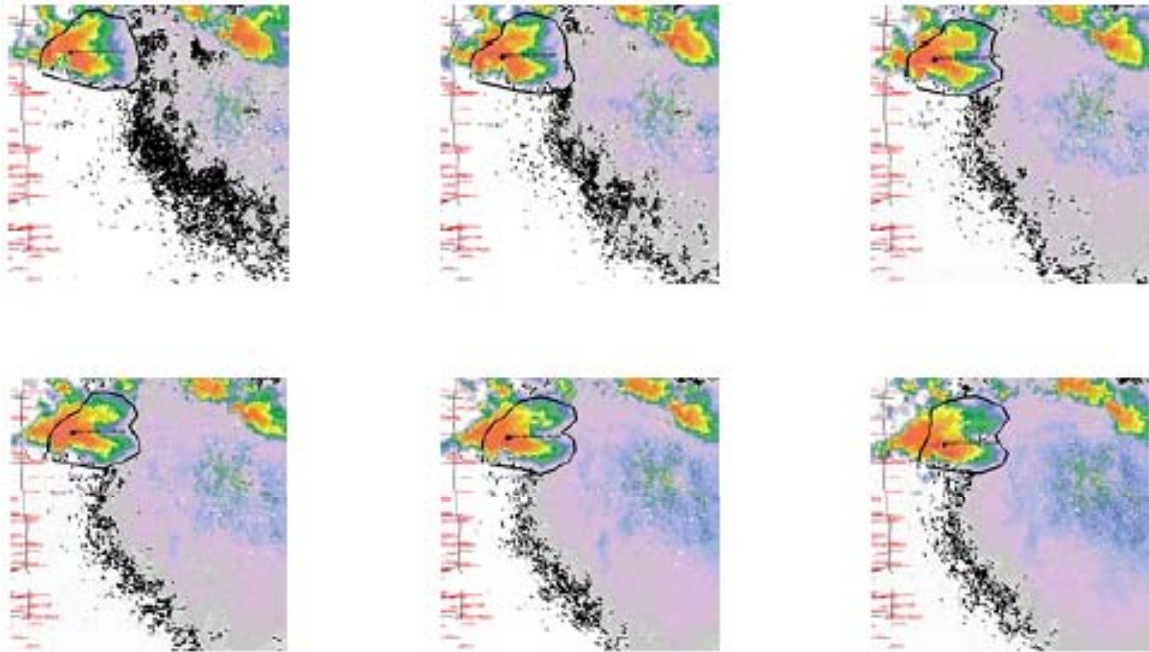
Figure A7. As in Fig. A1 but for Kaw Reservoir, OK, 7 May 1994, viewed from KINX between 0129 and 0329 UTC, for panels 1-45, respectively. Map height is 1.373 km AGL.
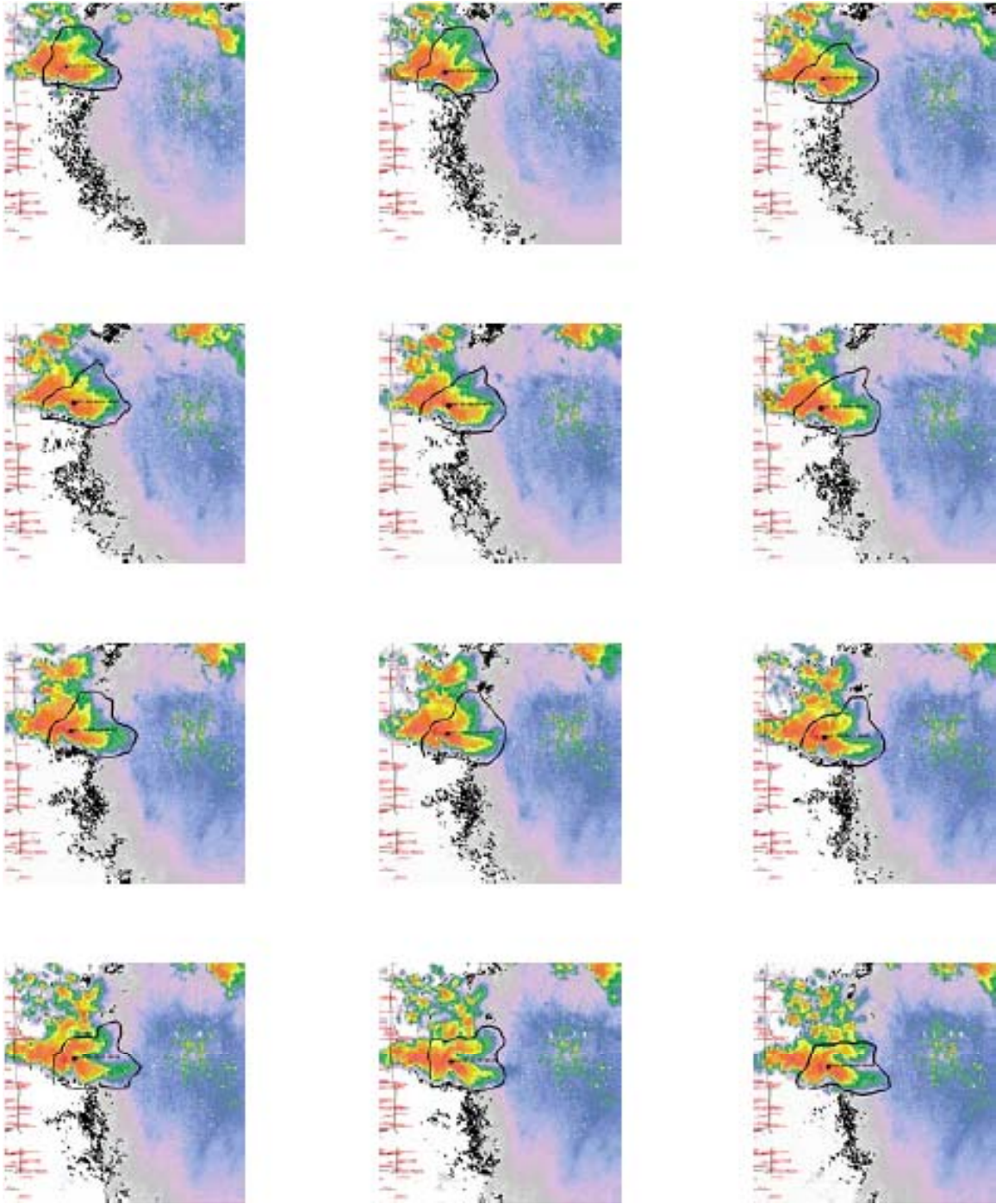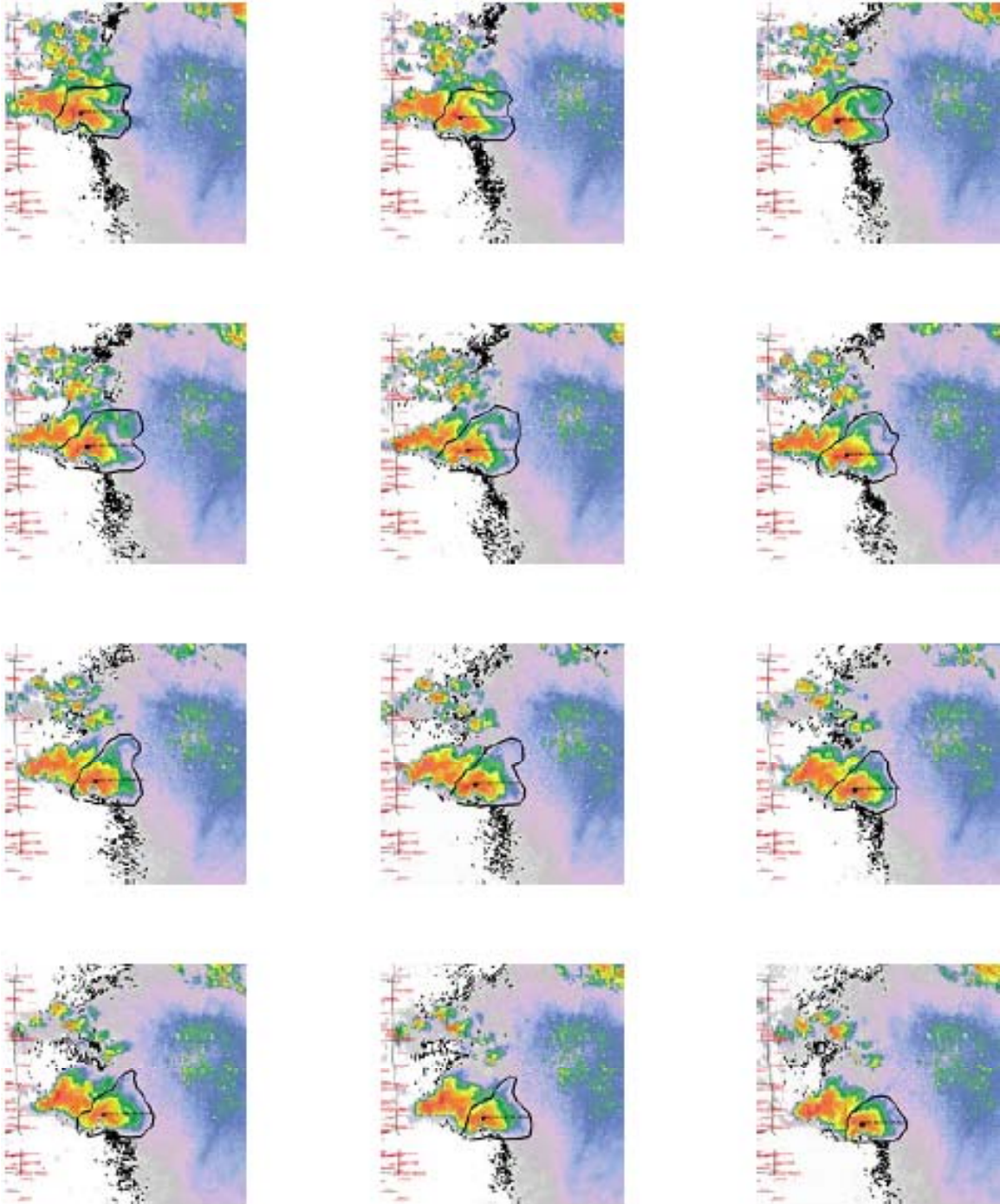
Figure A7. Continued. Panels 7-18.

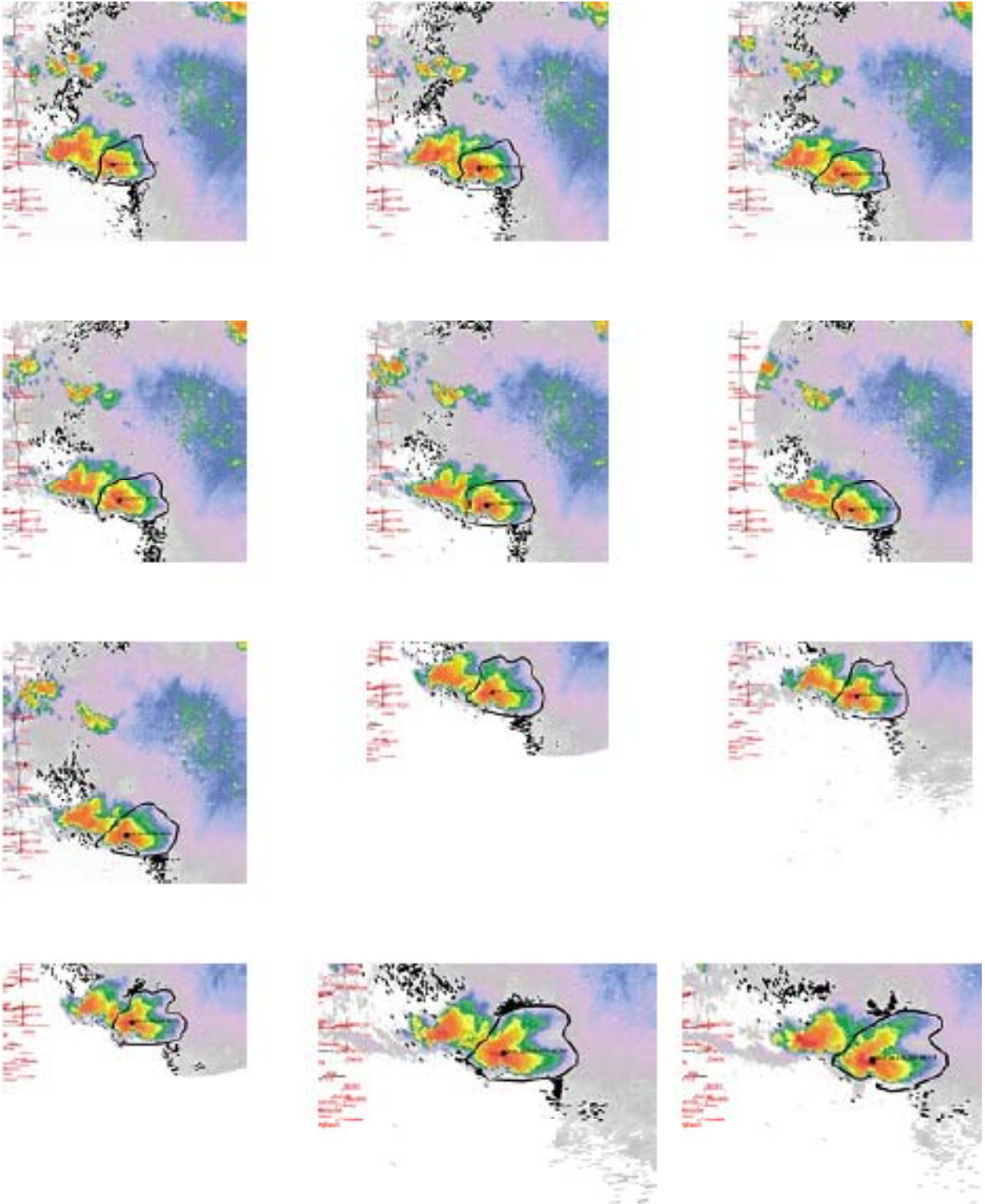Figure A7. Continued. Panels 19-30.
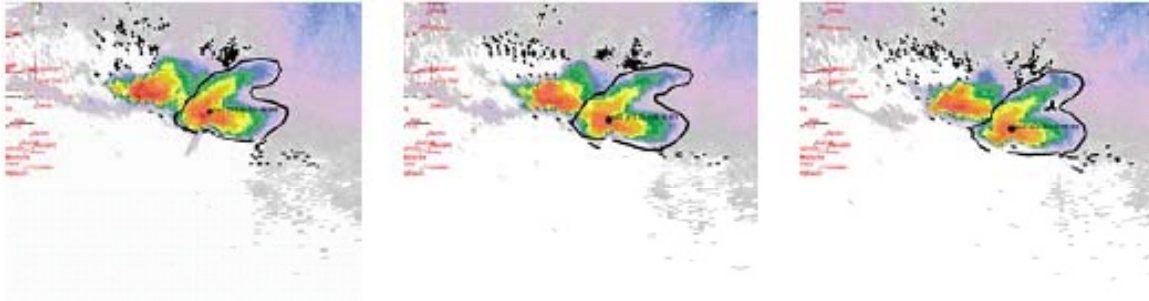
Figure A7. Continued. Panels 31-42.

<u>Figure A7</u>.   Continued. Panels 43-45.

REFERENCES

Barnes, S. L., 1964: A technique for maximizing details in numerical weather map analysis. *J. Appl. Meteor.*, **3**, 396-409.

Beatty, K., E. N. Rasmussen, and J. M. Straka, 2008: The supercell spectrum. Part I: A review of research related to supercell precipitation morphology. *Electronic J. Severe Storms Meteor.*, **3** (4), 1-21.

Brooks, H. E., C. A. Doswell III, and R. B. Wilhelmson, 1994: The role of midtropospheric winds in the evolution and maintenance of low-level mesocyclones. *Mon. Wea. Rev.*, **122**, 126-136.

Browning, K. A., 1978: The structure and mechanisms of hailstorms. *Hail: A Review of Hail Science and Suppression*, G. Foote and C. Knight, Eds., *Meteor. Monogr.*, No. 38, Amer. Meteor. Soc., 1-43.

Knight, C. A., and L. J. Miller, 1993: First radar echoes from cumulus clouds. *Bull. Amer. Meteor. Soc.*, **74**, 179-188.

Lemon, L. R., 1977: New severe thunderstorm radar identification techniques and warning criteria. NOAA Tech. Memo. NSSFC-3, 60 pp.

____, 1998: Updraft identification with radar. Preprints, *19th Conf. Severe Local Storms*, Minneapolis, MN, Amer. Meteor. Soc., 709-712.

____, and C. A. Doswell III, 1979: Severe thunderstorm evolution and mesocyclone structure as related to tornadogenesis. *Mon. Wea. Rev*., **107**, 1184-1197.

____, and D. W. Burgess, 1993: Supercell associated deep convergence zone revealed by a WSR-88D. Preprints, *26th International Conf. on Radar Meteorology*, Norman, OK, Amer. Meteor. Soc., 206-208.

____, and S. Parker, 1996: The Lahoma storm deep convergence zone: Its characteristics and role in storm dynamics and severity. Preprints, *18th Conf. on Severe Local Storms*, San Francisco, CA, Amer. Meteor. Soc., 70-75.

Marshall, J. S. and W. M. K. Palmer, 1948: The distribution of raindrops with size, *J. Meteor.* **5**, 165-166.

Marwitz, J. D., 1972a: The structure and motion of severe hailstorms. Part III: Severely sheared storms. *J. Appl. Meteor.*, **11**, 189-201.

____, 1972b: Locating the organized updraft in severe thunderstorms. *J. Appl. Meteor.*, **11**, 236-238.

Rasmussen, E. N., and J. M. Straka, 1998: Variations in supercell morphology. Part I: Observations of the role of upper-level storm-relative flow. *Mon. Wea. Rev.*, **126**, 2406-2421.

Speheger D. A., C. A. Doswell III, and G. J. Stumpf, 2002: The tornadoes of 3 May 1999: Event verification in central Oklahoma and related issues. *Wea. Forecasting*, **17**, 362–381.

Vieux, B. E., and P. B. Bedient, 1998: Estimation of rainfall for flood prediction from WSR-88D reflectivity: A case study, 17-18 October 1994. *Wea. Forecasting*, **13**, 126-134.

REVIEWER COMMENTS

[Authors' responses in *blue italics.*]

REVIEWER A (Donald W. Burgess):

Initial Review:

Recommendation: Accept with major revisions

General Comments:

General Comments: The ideas presented in the manuscript are good science and worthy of publication. I think the points about the similarity between LP and classic supercells are very important and could lead to major rethinking about supercell types…perhaps, just having two types: classic (which includes LP; Forward Reflectivity (FR) mode) and HP (Rear Reflectivity (RR) mode). However, the manuscript is not well written. It reads like an in-progress draft. Some good things are included, but lots of loose ends and potential dead ends need to be cleaned up before the manuscript would be ready for publication. Did the authors really review the manuscript and think it was ready for submission? This is not the first rodeo for any of these authors, and I'm surprised (and disappointed) that they would review this manuscript and think (in its present form) that it was ready for submission. As a reviewer, I would rather spend my review time commenting on the science, not commenting on all the little problems that are normally taken care of before submission.

Major Comments: Besides the accumulation of all the draft-not-ready-for-submission issues mentioned above (and listed below), I only have one other major comment about the manuscript. That is, mention of the current classification method being a candidate for automation is over-done. In my opinion, there is no way to automate the current technique. Quoting the authors' own words, at each step they mention that the step has lots of subjectivity: Step 1 (precip core location) – "parts of the method rely on human assessment (Pg 2);" and Step 2 (estimation of the low-level updraft location) – detection of WER, BWER, hook, concave, high-gradient reflectivity contours, updraft on inflow flank, and quality check to make sure the updraft location is in the correct place (all on Pg 4) are all subjective…and too much to currently envision automating. The title says "semi-objective" and I can go with that. The abstract says "objective" radar analysis and "could possibly be automated," I can't go with either of those phrases. I suggest wording changes to be made to the Abstract and Discussion/Conclusions (Section 4) to reflect the unlikely automation at any time in the foreseeable future. The Introduction comment ("someday it might be possible…objective and fully automated") seems OK to me…we can all wish for someday. Also, comments in Section 4 might include suggesting that future researchers come up with comparable steps that could be automated and/or used in real time.

We apologize for the distraction caused by the issues the reviewer characterized as "not ready for submission". Sometimes, there is a tradeoff between readability and flow, and complete precision, and sometimes authors assume that meanings are clear even when the verbiage is not complete and precise. But we have taken the reviewer's concerns to heart, and modified the text accordingly.

Further, we did let our enthusiasm for contributing to operations carry us a bit too far. The science is what is important here; the reviewer is correct. We endeavored to remove any wording or "flavor" of potential automation and algorithms. We hope our work catches the imagination of someone who can carry it onward. And we further hope that others will recognize the significance of the simple finding of forward vs. rearward centroid location, and perhaps seek to automate this indicator in ways that we haven't considered.

[Minor comments omitted...]

Second review:

General Comments: The ideas presented in the manuscript are good science and worthy of publication. The second submission is much improved. The flow of the manuscript is improved, and many of the problems that plagued the first submission have been fixed. I particularly liked the enlarging of the figure panels in the appendix. Unfortunately, there remain a number of minor comments that need to be addressed. I think the authors are very capable of making the remaining changes that need to be made. I will leave any possible further review steps to the good judgment of the editor. The figures are improved, but there are a few figure comments listed below. I will let the editor decide about what's best for the figures.

Major Comments: My previous concerns about the current classification method being a candidate for automation have been addressed in the second submission.

[Minor comments omitted...]

REVIEWER B (Arthur Witt):

Initial Review:

Reviewer recommendation: Accept with minor revisions

Substantive Comments: Overall, the paper is well written and easy to follow. However, the Methodology section needs clarification in several areas [see (minor) comments in the manuscript]. Also, most acronyms are not defined (I assume it's the policy of the EJSSM that all acronyms need to be defined), and some references are missing (or listed and not mentioned in the paper).

References and acronyms have been added and defined, respectively

[Minor comments omitted...]

REVIEWER C (Jay Martinelli):

Initial Review:

Recommendation: Accept with minor revisions

General Comments: The authors evaluate several case studies in an attempt to promote a new classification scheme for supercells based upon partially objective and partially subjective analyses. Their cases thus far clearly indicate two classes of supercells; those with supercell precipitation centroids located upstream of the updraft core (rear-reflectivity core) or those with supercell precipitation centroids located downstream of the updraft core (forward-reflectivity core).

Substantive Comments: I applaud your effort do develop a more robust classification scheme. I believe the research presented here shows promise for doing just that. I agree with the authors that developing a way to automate this technique is paramount to maximizing its utility.

It seems to me that the situations where it is most difficult to categorize supercells (interacting and close proximity), this technique would be difficult to apply. However, in cases where the supercell is isolated, it would not be needed.

For the current reader, what if anything can they do to utilize your findings?

They can differentiate a forward flank precipitation dominated storm from a rear flank precipitation dominated storm.

Concerning the SR wind data, what was the methodology employed to ensure that you were using representative profiler data?

(We) used typical proximity sounding criteria [Rasmussen and Blanchard (199)8 and others.]

[Minor comments omitted...]

Second review:

Recommendation: Accept

General Comments: I reread the manuscript and it looks fine. I had relatively minor concerns to begin with and they were addressed in the revision.